Research on D-Shape Open-Loop PCF Temperature Refractive Index Sensor Based on SPR Effect

Fanlong Meng [ID], Hong Wang [ID], and Di Fang [ID]

Abstract—PCF (Photonic crystal fiber) temperature refractive index sensor based on SPR effect with the new double membrane open-loop structure is proposed. The inner surface of such PCF's open-loop structure is plated with a layer of 70 nm gold film, and a layer of 20 nm SiO$_2$ film is coated on the gold film, which could effectively prevent the gold film from oxidation corrosion. Besides, the open loop could reduce the production cost, and it could form two energy channels with nearby air holes, promoting the leakage of core energy to plasma mode and enhancing the SPR effects. The ethanol could be adopted as the temperature sensing solution, to measure the refractive index sensing of the solution to be measured. Numerical simulation is carried out based on the full vector finite element method, and the simulation results indicate that the average wavelength sensitivity of refractive index sensing could reach 3330 nm/RIU, and the wavelength sensitivity of temperature sensing could reach 0.912 nm/° C, and a maximum figure of merit (FOM) of 102 which is approximately four times larger than that of the similar reported PCF-SPR sensors in the literature. The simulation results show that D-shape open-loop photonic crystal fiber has the potential application prospect on the temperature and refractive index sensing.

Index Terms—Finite element method, photonic crystal fiber (PCF), refractive index sensor, surface plasmon resonance (SPR), temperature sensor.

I. INTRODUCTION

SINCE its advent, the photonic crystal is widely applied in the sensor, filter, all-optical switch [1]–[3] and other optical device. In 1902, Wood found [4] that when the polarized light source continuously irradiates a metal grating, there will be a narrow dark band in the diffraction spectrum. In 1960, Stern and Ferrell officially put forward the concepts of SP and SPR [5]. SPR effect is essentially a plasma optical excitation effect and the polarized light generates the electronic shock at the junction of metal and dielectric so as to generate the plasma resonance effect. Besides, the surface plasma is sensitive to the refractive index change of the surrounding environment. Refractive index of photonic crystal fiber and temperature sensor based on the surface plasmon resonance (SPR) shall realize the sense with the high sensitivity and high resolution [6], [7]. In 2014, Guan *et*

al. [8] designed the double-film six-air-hole single-mode optical fiber SPR sensor. Its maximum sensitivity is 370 RIU^{-1} and resolution ratio is 2.7×10^{-5} RIU. In 2016, Ayyanar *et al.* [9] designed the asymmetric double elliptical core PCF based on liquid filling, and 42.99 nm/° C high-sensitivity temperature sensing could be realized with the short length. In 2019, Zhao *et al.* [10] designed one all-solid-state D-shape PCF based on the SPR effect, which could measure the refractive index and temperature of liquid. Its measuring rage falls $-3 - 15°$C and the maximum temperature sensitivity could reach 4.22 nm/°C. When the measuring range of refractive index falls in 1.41–1.42, the sensitivity of the maximum refractive index could reach 10300 nm/RIU. At present, most of the D-type PCF gold film are directly connected to the solution and it is prone to be oxidized and corroded by the solution to be measured. Besides, to realize the temperature sensing, the traditional D-type PCF needs to fill the temperature sensitive liquid to the nanoscale air holes, but it is not easy to achieve in the reality. Hence, to prevent the gold film from the corrosion by the solution to be measured, enhance the SPR effects, simplify the preparation process and reduce the production cost, this paper proposes the PCF-SPR sensor with elliptical open-loop double-layer membrane structure, and the gold film is coated on the inner surface of the elliptical open loop. Then, a layer of SiO$_2$ film is applied, which could effectively prevent the gold film from oxidation. It also does not affect the SPR effects in PCF. The open-loop structure could avoid the complex procedure of the liquid filling, reduce the production costs and form two energy channels with nearby air holes, promoting the leakage of core energy to plasma mode and enhancing the SPR effects. Compared with the D-PCF with a hexagonal lattice of air holes, the D-PCF we proposed has two passageway to let the core-mode light couple with the SPP mode. It can help us increase the sensitivity of the sensor. The analyte can flow through this channel and filter some impurities larger than the opening. The simulation results show that the refractive index of analytical solution falls on 1.35–1.40, the average wavelength sensitivity of the sensor is 3330 nm/RIU, the temperature measurement range is 20–60° C and the sensitivity is 0.912 nm/°C.

II. THEORETICAL RESEARCH MODEL

Cross section of D-shape elliptic open loop PCF designed is shown in Fig. 1. The existence of open loop can make more analyte volume interact with the core light guide, which enhances the wide-range refractive index coupling of analyte,

Fig. 1.   Schematic diagram of photonic crystal fiber section.

Fig. 2.   Dispersion relationship of the y-polarization core mode (black), SPP mode (blue), and loss spectrum (red).

when the sample flows into the open loop, it can filter out the impurities larger than the open loop in the sample.

The diameter of the first-layer large circular air hole away from the fiber core is d $_1$ = 1.6μ m, the diameter of the small circular air hole near the fiber core is d $_2$ = 0.8μ m, the long axis of the elliptical air hole is a = 1.2μm, the short axis is b = 0.8μm, and the hole spacing is Λ = 2.3μm. The golden part on the innermost side of the open-loop ellipse is a metal layer with a thickness of m$_1$ = 70 nm, and the outermost side of the open-loop is a SiO$_2$ layer with a thickness of m$_2$ = 20 nm. The blue part is the solution RI to be measured, and the outermost dark gray ring is the perfect matching layer. According to Drude-Lorentz, the dielectric constant of Au [11]:

$$\varepsilon_{Au}(\omega) = \varepsilon_1 + i\varepsilon_2 = \varepsilon_\infty - \frac{\omega_p^2}{\omega(\omega + i\omega_c)} \quad (1)$$

where in, the dielectric constant of Au is $\varepsilon_\infty = 9.48$, the plasma angular frequency is $\omega = 1.36 \times 10^{16} rad/s$. Temperature sensitive liquid adopts ethanol solution and its refractive index changes with the temperature [12] could be expressed as:

$$n = n_0 - \frac{dn}{dT}(T - T_0) \quad (2)$$

where in, the refractive index of the ethanol solution is $n_0 = 1.36048$ at 20°C and the thermal coefficient of ethanol is $\frac{dn}{dT} = 3.94 \times 10^{-4}$. The base material is fused quartz, and its material dispersion can be obtained from Sellmeier equation [13]:

$$n^2_{sio_2} = 1 + \frac{B_1\lambda^2}{\lambda^2 - C_1} + \frac{B_2\lambda^2}{\lambda^2 - C_2} + \frac{B_3\lambda^2}{\lambda^2 - C_3} \quad (3)$$

they are the wavelength of incident light, and B$_1$, B$_2$, B$_3$, C$_1$, C$_2$, C$_3$ are the constant of Sellmeier.

III. RESULTS AND ANALYSIS

Working principles of the sensor are that the evanescent wave generated by the incident light at the total reflection of the optical fiber interacts with the metal surface and it excites the plasma wave at the metal surface. When the phase matching
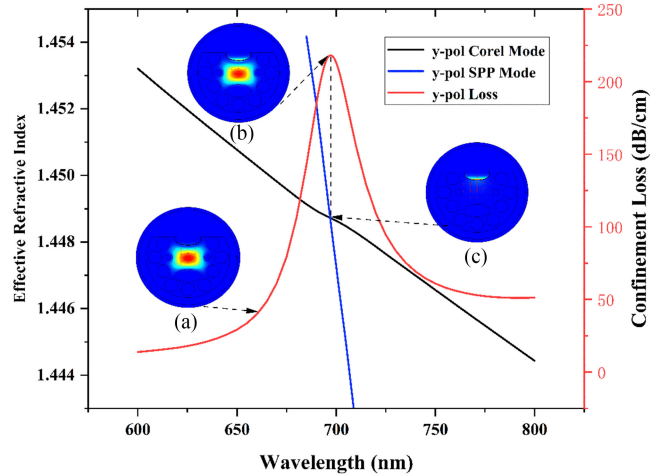
TABLE I
COMPARISON TABLE OF PROPOSED SENSOR WITH SOME OTHER SENSOR

Ref	RI Sensing Rang	Average Sensitivity (nm/RIU)	Plasmonic Material
[16]	1.27-1.37	2320	Graphite on silver
[17]	1.34-1.36	3700	Ag
[18]	1.33-1.35	2520	Ag and graphene
[19]	1.27-1.36	2350	Gold
This work	1.35-1.40	3300	Silica on gold

occurs with the plasma wave, the incident light energy is largely absorbed by electrons on the metal surface, and it generates the SPR effect, so the fundamental mode loss of the optical fiber is the largest and the incident light wavelength is called as the resonance wavelength. When the temperature changes, the refractive index of temperature sensitive liquid will also change, so as to change the resonance wavelength. By studying the loss peak of the polarization mode and shift of resonance wavelength, the temperature and RI test will be realized. The simulation process is accomplished by the commercial finite element method [14] solver-COMSOL Multiphysics 5.6. The grid sequence type is to control the grid with physical field, and the grid size is set to general. As shown in Fig. 2, when the temperature is 20°C and the incident light wavelength changes from 600 nm to 800 nm, the variation curve of the loss of the basic mode of the temperature sensor is related to the effective refractive index of the core base mode and SPP mode. When the incident light wavelength is 697 nm, the loss of core base mode is the largest and the loss peak occurs with the peak value of 218.79 dB/cm. Loss value of core base mode could be obtained via (4) [15]:

$$\alpha_{loss}\left(\frac{dB}{cm}\right) = 8.686 \times \frac{2\pi}{\lambda} \times Im(n_{eff}) \times 10^4 \quad (4)$$

where in, $Im(n_{eff})$ is the imaginary part of the effective refractive index of the core fundamental mode. Inset (a) shows the core mode at 610 nm, inset (b) shows the core mode at 697 nm, and inset (c) shows the SPP mode at 697 nm.
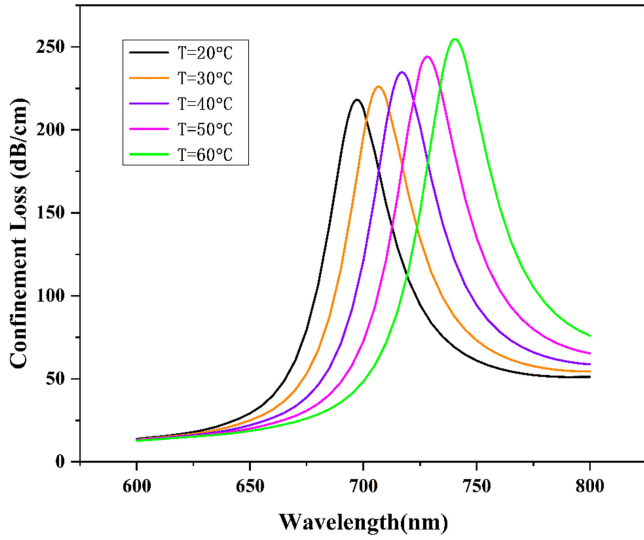
Fig. 3. Dependence of the confinement loss curve of the y-polarized on the analyte temperature.

Fig. 4. Variation of amplitude sensitivity for temperature change of $10°C$.

A. The Temperature Sensor

When the temperature changes, the refractive index of temperature sensitive liquid ethanol will also change and the refractive index is determined by the formula (2). It changes will also change the resonance wavelength and loss peak, and the loss curve under different temperatures is shown in the Fig. 3 as follows. Based on the boiling point of the ethanol solution, the temperature measurement range of the sensor is fixed in 20–60°C. When the temperature is at 20°C, 30°C, 40°C, 50°C and 60°C, the ethanol's refractive index will be 1.3604, 1.3644, 1.3684, 1.3723 and 1.3762, respectively. With the temperature increasing, the ethanol's refractive index will be greater. The loss of fundamental mode increases and the resonance wavelength increases gradually.

Based on the above research, the sensitivity of the sensor's temperature could be defined by the formula (5):

$$S_T \left(\frac{nm}{°C} \right) = \frac{\Delta\lambda_{peak}}{\Delta T} \quad (5)$$

where in, $\Delta\lambda_{peak}$ is the offset of resonance wavelength and ΔT is the temperature change. When the temperature increases to 60°C from 20°C, the offset of loss peak is 10 nm, 10 nm, 11 nm and 12 nm for each increase of 10°C, and the wavelength sensitivity according to the formula (5) is 1 nm/°C, 1 nm/°C, 1.1 nm/°C and 1.2 nm/°C, respectively. It could be known that the variation of temperature is almost linear with the shift of resonance wavelength. In addition, the radiance sensitivity is the important performance parameter. Its definition equation:

$$S \left(RIU^{-1} \right) = -\frac{1}{\alpha(\lambda, n_a)} \frac{\partial_\alpha(\lambda, n_a)}{\partial n_a} \quad (6)$$

where in, $\alpha(\lambda, n_\alpha)$ is the fundamental mode loss of the optical fiber, $\partial_\alpha(\lambda, n_a)$ is the difference between the fundamental mode losses at two adjacent temperatures, and ∂n_a is the difference of the refractive index of the material to be measured. Fig. 4 is
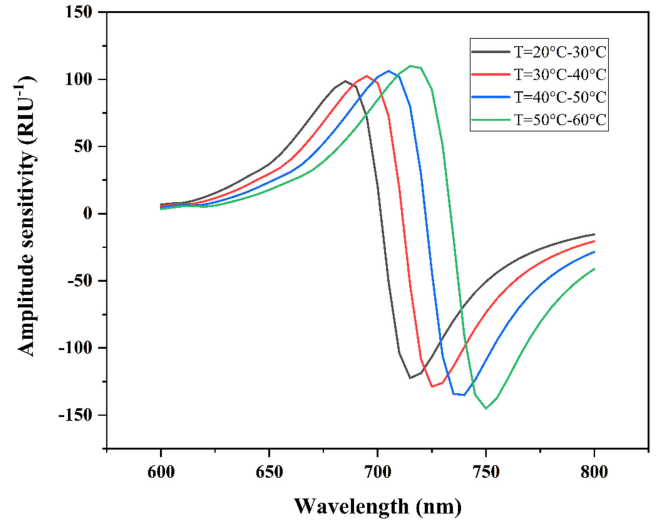
the variation curve of radiance sensitivity from 20°C to 60°C. It could be found that, when the temperature falls in 20°C $-30°$ C, 30°C $-40°$ C, 40°C-50°C and 50°C $-60°$ C, the available maximum radiance sensitivity is 122.37 RIU $^{-1}$,128.74 RIU^{-1},135.03 RIU^{-1} and 145.1 RIU^{-1},and the corresponding wavelength of maximum radiance sensitivity is 715 nm, 725 nm, 740 nm and 750 nm, respectively.

B. Refractive Index Sensor

When the ambient temperature is unchanged, the loss peak of the solutions with different refractive indexes varies, so the refractive index of the solution to be measured could be obtained by observing the loss peak transfer in PCF or change of the resonance wavelength, which is the principles of the refractive index sensing. When the temperature is 20°C, the corresponding fundamental mode loss curve is shown in the Fig. 5 after changing the refractive index of the solution to be measured. When the refractive index is 1.35, 1.36, 1.37, 1.38, 1.39 or 1.40, the wavelength of the corresponding fundamental mode loss peak is 696 nm, 722 nm, 753 nm, 794 nm or 849 nm, respectively.

$$S_n \left(\frac{nm}{RIU} \right) = \frac{\Delta\lambda_{peak}}{\Delta n_a} \quad (7)$$

where in, $\Delta\lambda_{peak}$ is the change of the resonance wavelength in the core loss spectrum with the refractive index of the solution to be measured, and Δn_α is the change of the refractive index of the solution to be measured. When the refractive index of the solution to be measured is 1.35–1.40, for every increase of 0.01, the corresponding wavelength offset of the loss peak is 21 nm, 26 nm, 31 nm, 41 nm and 55 nm, respectively. According to the formula (7), the corresponding wavelength sensitivity is 2100 nm/RIU, 2600 nm/RIU, 3100 nm/RIU, 4100 nm/RIU and 5100 nm/RIU, respectively. The overall performance of a PCF-SPR sensor can be evaluated with a figure of merit (FOM) parameter. FOM in spectral-based SPR sensors is usually defined as the ratio between sensitivity and FWHM of the
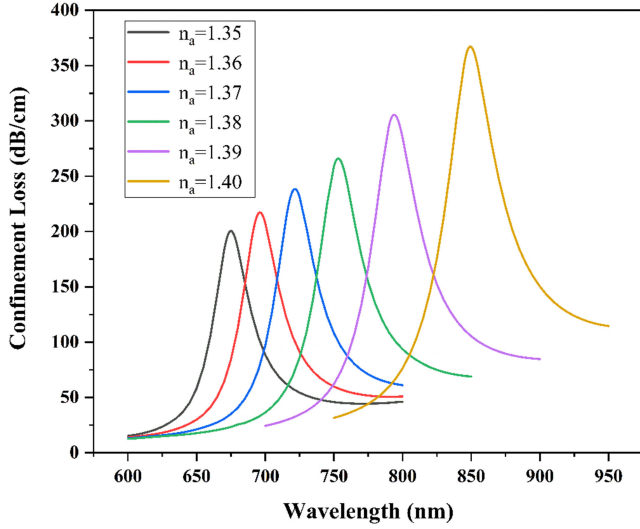
Fig. 5. Dependence of the confinement loss curve of the y-polarized on the analyte RI.
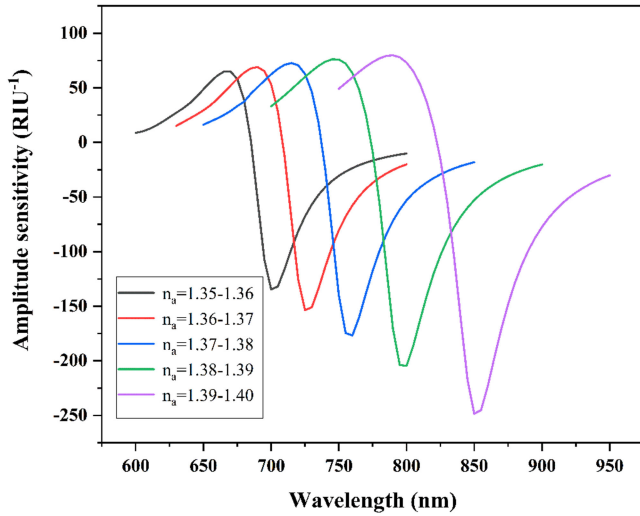

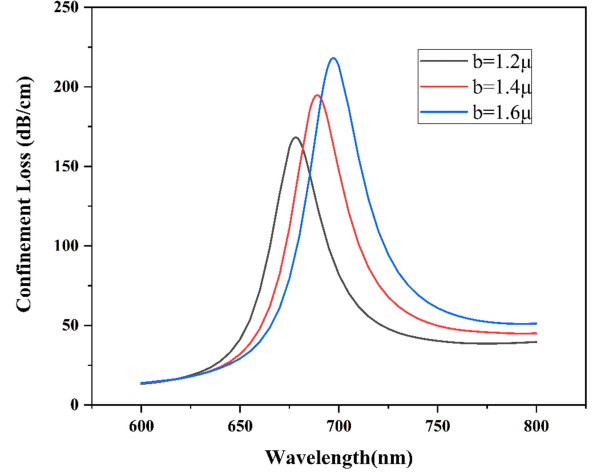Fig. 6. Variation of amplitude sensitivity for RI change of 0.01.

Fig. 7. Dependence of the confinement loss curve of the y-polarized on the ellipse major axis b.
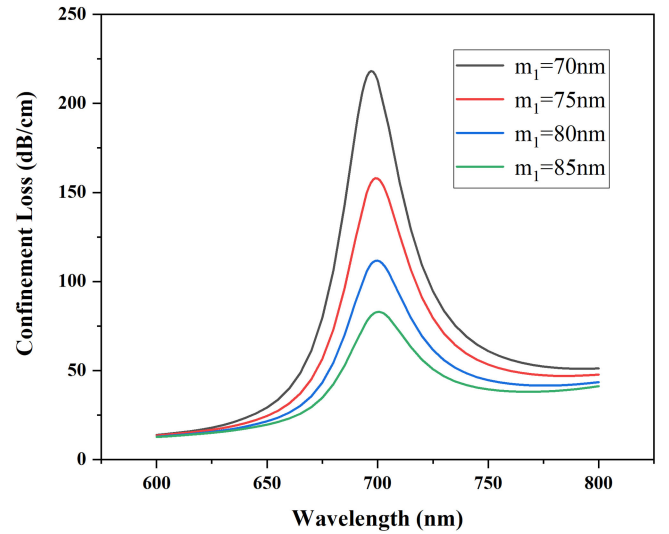
Fig. 8. Loss curves of the proposed SPR-PCF sensor for different gold film thickness m_1.

peak [16], the optimal value of FOM in this paper is 102 RIU^{-1}.

$$FOM = S_{spectral}(nm/RIU)/FWHM_{peak}(nm) \qquad (8)$$

The corresponding radiance sensitivity of the refractive index sensing is shown in the Fig. 6. When the refractive index of solution to be measured is 1.35–1.36, 1.36–1.37, 1.37–1.38, 1.38–1.39 and 1.39–1.40, the available maximum radiance sensitivity is 134.64 RIU^{-1}, 153.51 RIU^{-1}, 176.61 RIU^{-1}, 204.59 RIU^{-1} and 248.41 RIU^{-1}, respectively. The corresponding wavelength of the maximum radiance sensitivity is 700 nm, 725 nm, 760 nm, 800 nm and 850 nm.

C. Influence of PCF Structure on Sensor Performance

Air hole in RCF is the important parameter index of the sensor. It could not only limit the transmission of incident light in the fiber core, but also meet the plasma resonance effect between the fundamental mode and the metal layer. This paper focuses on simulating the impact of the long-axis radius of the elliptical air hole on the performance of fiber sensor. As shown in Fig. 7, when the long-axis b of the elliptical air hole is 1.2 μm, 1.4 μm and 1.6 μm, the loss curve of the fundamental mode of optical fiber will change. The resonance wavelength will increase with the extension of the long-axis radius of ellipse, and the loss peak increases gradually. With the enlargement of ellipse air hole, the gold film area increases, which promotes the leakage of the fiber core energy to the plasma model and enhances the SPR resonance effect.

The thickness of gold film has a large impact on the sensing performance. If the gold film is too thick, the sensitivity and the peak loss will be significantly reduced, as the electric field cannot penetrate through the gold layer. While if the gold film is too thin, the plasmonic wave will be strongly damped because of radiation damping. Fig. 8 exhibits the loss spectra variations for different goldfilm thickness m_1 ranging from 70 nm to 85 nm.

As is shown, when the thickness of gold film increases from 70 nm to 85 nm, the loss of core fundamental mode decreases sharply from 218.18 dB/cm, and the full width at half peak of resonance peak increases greatly. And we can also notice that the loss spectra of $m_1 = 70$ nm has a sharper resonance peak, thus $m_1 = 70$ nm might be an optimized gold film thickness.

D. Comparative Discussion

A comparison is shown in Table I based on average sensitivity and RI sensing range. All the other references are proposed designs of PCF SPR sensors, based on FEM, whose results have been numerically investigated. It is concluded that the proposed sensor has better average sensitivity than other existing sensors in references [16]–[19].

IV. CONCLUSION

This paper proposes and verifies the oval open-loop structure SPR-PCF sensor, and measure the external temperature and solution refractive index. Compared with the D-PCF with a hexagonal lattice of air holes, the D-PCF we proposed has two passageway to let the core-mode light couple with the SPP mode. It can help us increase the sensitivity of the sensor. The elliptical open loop could construct two energy transmission channel with the surrounding cladding air holes, which promotes the leakage of the core fundamental mode energy to the plasma model and greatly enhances the SPR effects. SiO_2 film coated outside gold film could effectively prevent the gold film oxidation, and do not affect the sensor measurement. In the temperature range of $20°C - 60°C$, the sensitivity is 0.912 nm/$°C$. When the refractive index of analysis solution is 1.35–1.40, the average wavelength sensitivity of the sensor is 3330 nm/RIU. The research is of great significance to the research and development of the temperature sensing field.

REFERENCES

[1] A. Mohamadi, M. Seifouri, R. Karami, and S. Olyaee, "Proposal of a high-Q biosensor using a triangular photonic crystal filter," *Opt. Quantum Electron.*, vol. 53, no. 8, pp. 1–12, 2021.

[2] S. Khani, M. Danaie, and P. Rezaei, "Hybrid all-optical infrared metal-insulator-metal plasmonic switch incorporating photonic crystal bandgap structures," *Photon. Nanostructures-Fundamentals Appl.*, vol. 40, 2020, Art. no. 100802.

[3] A. Panda and P. D. Pukhrambam, "Analysis of GAN-based 2D photonic crystal sensor for real-time detection of alcohols," *Braz. J. Phys.*, vol. 51, no. 3, pp. 481–492, 2021.

[4] R. W. Wood, "XIII. on a remarkable case of uneven distribution of light in a diffraction grating spectrum," *London, Edinburgh, Dublin Philos. Mag. J. Sci.*, vol. 4, no. 21, pp. 396–402, 1902.

[5] C. Powell and J. Swan, "Effect of oxidation on the characteristic loss spectra of aluminum and magnesium," *Phys. Rev.*, vol. 118, no. 3, 1960, Art. no. 640.

[6] A. Hassani and M. Skorobogatiy, "Design of the microstructured optical fiber-based surface plasmon resonance sensors with enhanced microfluidics," *Opt. Exp.*, vol. 14, no. 24, pp. 11616–11621, 2006.

[7] S.K. Srivastava and B. D. Gupta, "Simulation of a localized surface-plasmon-resonance-based fiber optic temperature sensor," *J. Opt. Soc. Amer. A*, vol. 27, no. 7, pp. 1743–1749, 2010.

[8] D. Gao, C. Guan, Y. Wen, X. Zhong, and L. Yuan, "Multi-hole fiber based surface plasmon resonance sensor operated at near-infrared wavelengths," *Opt. Commun.*, vol. 313, pp. 94–98, 2014.

[9] N. Ayyanar, R. V. J. Raja, D. Vigneswaran, B. Lakshmi, M. Sumathi, and K. Porsezian, "Highly efficient compact temperature sensor using liquid infiltrated asymmetric dual elliptical core photonic crystal fiber," *Opt. Mater.*, vol. 64, pp. 574–582, 2017.

[10] L. Zhao, H. Han, Y. Lian, N. Luan, and J. Liu, "Theoretical analysis of all-solid d-type photonic crystal fiber based plasmonic sensor for refractive index and temperature sensing," *Opt. Fiber Technol.*, vol. 50, pp. 165–171, 2019.

[11] M. R. Hasan *et al.*, "Spiral photonic crystal fiber-based dual-polarized surface plasmon resonance biosensor," *IEEE Sensors J.*, vol. 18, no. 1, pp. 133–140, Jan. 2018.

[12] Y. Yu *et al.*, "Some features of the photonic crystal fiber temperature sensor with liquid ethanol filling," *Opt. Exp.*, vol. 18, no. 15, pp. 15383–15388, 2010.

[13] G. Ghosh, M. Endo, and T. Iwasaki, "Temperature-dependent sell-meier coefficients and chromatic dispersions for some optical fiber glasses," *J. Lightw. Technol.*, vol. 12, no. 8, pp. 1338–1342, 1994.

[14] Y. Zhou *et al.*, "Asymmetric double-core fiber for hydraulic pressure sensing," *Opt. Fiber Technol.*, vol. 48, pp. 194–198, 2019.

[15] J. Villatoro, E. Antonio-Lopez, J. Zubia, A. Schülzgen, and R. Amezcua-Correa, "Interferometer based on strongly coupled multi-core optical fiber for accurate vibration sensing," *Opt. Exp.*, vol. 25, no. 21, pp. 25734–25740, 2017.

[16] Y. Esfahani Monfared and M. Qasymeh, "Plasmonic biosensor for low-index liquid analyte detection using graphene-assisted photonic crystal fiber," *Plasmonics*, vol. 16, no. 3, pp. 881–889, 2021.

[17] D. Santos, A. Guerreiro, and J. M. Baptista, "SPR optimization using meta-materials in a D-type PCF refractive index sensor," *Opt. Fiber Technol.*, vol. 33, pp. 83–88, 2017.

[18] X. Yang, Y. Lu, B. Liu, and J. Yao, "Analysis of graphene-based photonic crystal fiber sensor using birefringence and surface plasmon resonance," *Plasmonics*, vol. 12, no. 2, pp. 489–496, 2017.

[19] C. Liu *et al.*, "Analysis of a surface plasmon resonance probe based on photonic crystal fibers for low refractive index detection," *Plasmonics*, vol. 13, no. 3, pp. 779–784, 2018.